NoiSER: Noise is All You Need for Enhancing Low-Light Images Without Task-Related Data

Zhao Zhang^{1*}, Suiyi Zhao¹, Xiaojie Jin², Mingliang Xu³, Yi Yang⁴, and Shuicheng Yan⁵

¹ Hefei University of Technology, Hefei, China

² Bytedance Research, USA

³ Zhengzhou University, Zhengzhou, China

⁴Zhejiang University, Hangzhou, China

⁵Sea AI Lab, Singapore

Abstract

This paper is about an extraordinary phenomenon. Suppose we don't use any low-light images as training data, can we enhance a low-light image by deep learning? Obviously, current methods cannot do this, since deep neural networks require to train their scads of parameters using copious amounts of training data, especially task-related data. In this paper, we show that in the context of fundamental deep learning, it is possible to enhance a low-light image without any task-related training data. Technically, we propose a new, magical, effective and efficient method, termed Noise SElf-Regression (NoiSER), which learns a gray-world mapping from Gaussian distribution for low-light image enhancement (LLIE). Specifically, a self-regression model is built as a carrier to learn a gray-world mapping during training, which is performed by simply iteratively feeding random noise. During inference, a low-light image is directly fed into the learned mapping to yield a normal-light one. Extensive experiments show that our NoiSER is highly competitive to current task-related data based LLIE models in terms of quantitative and visual results, while outperforming them in terms of the number of parameters, training time and inference speed. With only about 1K parameters, NoiSER realizes about 1 minute for training and 1.2 ms for inference with 600×400 resolution on RTX 2080 Ti. Besides, NoiSER has an inborn automated exposure suppression capability and can automatically adjust too bright or too dark, without additional manipulations.

1. Introduction

Unfavorable illumination is often encountered when taking photographs, and the resulted poorly illuminated photos greatly hinder understanding of their contents. Low-light image enhancement (LLIE) is a task that transforms low-light images into normal-light images, aiming at refining the

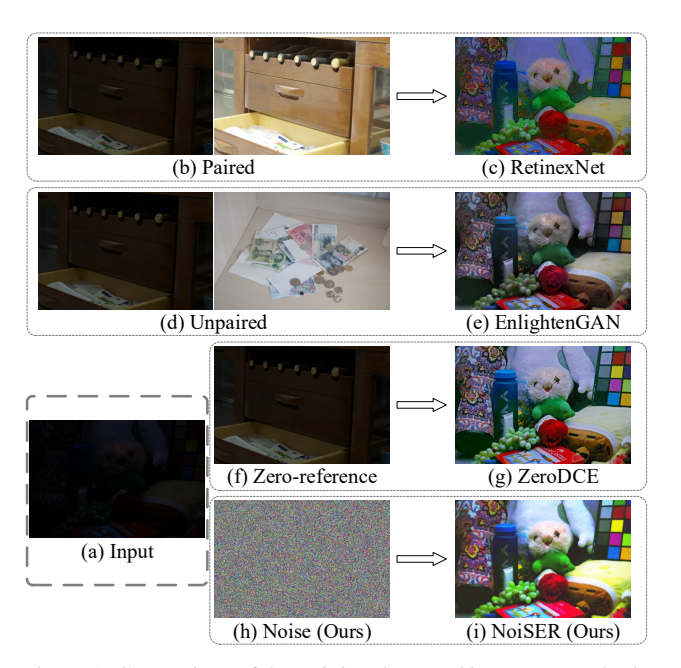


Figure 1. Comparison of the training data used in current methods, e.g., RetinexNet [33], EnlightenGAN [12] and Zero-DCE [8], and our proposed NoiSER. Clearly, the training data can be paired, unpaired, zero-reference and noise (in our NoiSER).

illuminations in low-light images. Recent years have witnessed significant progress for LLIE [8, 9, 33, 40] and have attracted much attention in emerging applications [31,43].

Traditional LLIE methods are mainly based on histogram equalization (HE) and retinex theory. The basic idea of HE-based methods is to widen the gray levels with a large number of pixels and to reduce the gray levels with a small number of pixels, so that the image can be enhanced. While retinex-based methods [9, 18, 33, 37] aim to estimate the illumination map to obtain reflectance (i.e., high-light image) based on the principle that low-light image can be decom-

posed into reflectance and illumination. Due to the inherent mechanisms of these methods, they will cause unpleasant artifacts and require a long processing time.

More recently, deep neural networks (DNNs) have been widely used for various computer vision tasks [3, 6, 23, 25, 27, 34, 36, 41, 42, 44] due to their strong ability to learn a general mapping from task-related training data. This also gives birth to advanced deep learning-based LLIE methods [8, 12, 15, 20, 35, 38–40], in which task-related data is a necessary condition.

Paired data, i.e., paired low-light and normal-light images (see Fig.1(b)), as strong LLIE-related data, are needed for supervised/semi-supervised models to obtain a powerful mapping to produce promising results [19, 38–40]. LL-Net [19] is a pioneering method to apply deep learning for LLIE by training an auto-encoder to extract features and enhance images. KinD [39] and KinD++ [38] are based on the retinex theory, which include three deep sub-networks to handle LLIE, obtaining remarkable results compared to other traditional retinex-based methods. DCC-Net [40] discusses the chromatic aberration phenomenon in LLIE, and proposes a "divide and conquer" strategy to enhance images while retaining image color. However, paired data are costly to be collected in reality. As such, synthetic paired data are usually used by current methods, which limits their practical applications due to the weak generalization ability caused by the large gap between synthetic and real data.

Unpaired data, i.e., non-corresponding normal-light and low-light images (see Fig.1(d)), as ordinarily LLIE-related data, are used for unsupervised models, such as [12]. EnlightenGAN [12] is based on generative adversarial networks (GAN) [7], which is the first to utilize fully unpaired data to train a GAN for unsupervised LLIE. Yet, these methods usually rely on a huge number of parameters to compensate for the weak constraints caused by unpaired data, which also hinders the practical applications of LLIE.

Zero-reference data, i.e., single low-light images only (see Fig.1(f)), as the weakly LLIE-related data, facilitate a simple and elegant LLIE model that trains a simple DNN by an elaborate unsupervised loss [8, 15, 18, 20]. Zero-DCE [8] and Zero-DCE++ [15] convert the LLIE task into deep curve estimation, and obtain visually pleasing enhancement results. RUAS [18] first introduces the neural architecture search (NAS) into LLIE task and searches out an efficient network structure for LLIE. SCI [20] develops a selfcalibrated illumination learning framework with remarkably enhanced results by taking into account the computational efficiency, flexibility and robustness. These methods yield surprising results using only zero-reference data, and meanwhile are far more lightweight and efficient than those methods using paired/unpaired data. However, the performance of these methods is highly dependent on training data and it is still hard to find the most suitable data.

It is worth noting that the data used in all aforementioned methods are task-related, no matter what they are strongly, ordinarily or weakly related, which is consistent with the accepted beliefs that task-related training data are always needed. So far, still no one tries to, or at least hasn't succeeded in training a deep model for a specific task with completely task-irrelevant data, but we did. We show that just using noise can also lead to surprising LLIE results. Specifically, we build a deep model as a carrier to learn a grayworld mapping, by just sampling the noise (see Fig.1(h)) from a Gaussian distribution as training data to fit the parameters. As a result, a low-light image can be easily enhanced via the learned mapping during inference. We summarize the main contributions as follows:

- To the best of our knowledge, unlike all the current deep learning paradigms, this is the first attempt to learn a general "generalization" directly from the task-irrelevant data, instead of the common "fit → generalize" procedure. Experiments show the solution to this new paradigm has strong generalization abilities, such as stable performance on different datasets, automated exposure suppression and brightness-adaptive.
- We propose a remarkably simple and effective unsupervised LLIE model, termed <u>Noise SElf-Regression</u> (NoiSER) via learning a gray-world mapping. Different from all existing LLIE methods, NoiSER is an amazing model, since it doesn't need any task-related data for training, and just uses the randomly sampled noise from Gaussian distribution to enable the training of the model, i.e., noise is all NoiSER needs for LLIE.
- On several benchmark datasets, our NoiSER yields the highly competitive to other competitors that used different types of task-related data quantitatively and qualitatively. Without any task-related data, NoiSER can recover the low-light images accurately in detail, naturalness and color, and most importantly, it has an automated ability to turn extreme light/dark into moderates due to the learned gray-world mapping. In addition, NoiSER is extremely lightweight and efficient in both training and inference phases. Specifically, with only about 1K parameters, NoiSER achieves about 1 minute for training and 1.2 milliseconds for inference on 600x400 resolution image by a single RTX 2080 Ti.

2. Preliminaries

2.1. Image Self-Regression Principle

Image self-regression describes a process whereby the input data itself acts as a supervised signal to reconstruct the output with the same size, which is based on deep learning and falls under the category of self-supervised learning. Assuming that we have a set of identically distributed data

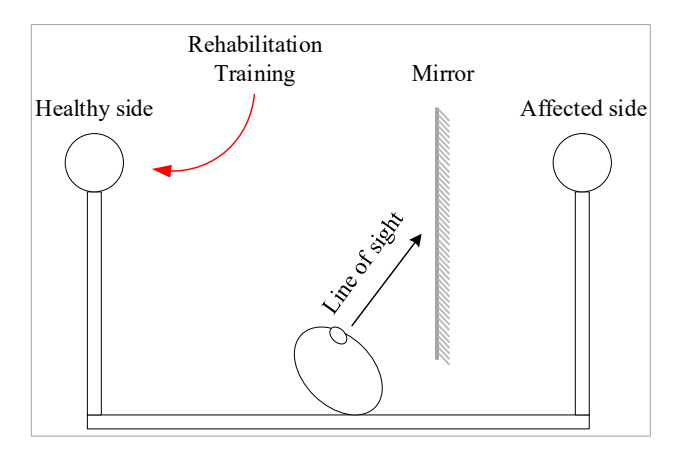


Figure 2. The schematic diagram of the MVF therapy (top view).

 $(x_1, x_2, ...)$, the image self-regression can be represented by minimizing the following empirical risk:

$$\underset{\theta}{\arg\min} \, \mathbb{E}_x \{ L(f_{\theta}(x), x) \}, \tag{1}$$

where f_{θ} represents a parametric family of mapping and L denotes a loss function.

In recent years, image self-regression has been applied as a learning approach to a variety of tasks, including dimensionality reduction [11], image generation [14] and image restoration [28], with significant and far-reaching impact. Deep image prior [28], as the most relevant self-regression method, uses the corrupted image as input and supervised signal to reconstruct the natural image, which obtains stunning results in multiple tasks, such as denoising, superresolution and inpainting, which means that a DNN has an innate ability to learn the "uncorrupted, natural" part of the image before it learns the "corrupted" part.

2.2. Gray-World Color Constancy Hypothesis

The gray-world color constancy hypothesis [1] (shortly, gray-world hypothesis) is a significant theory in image processing, which tells: for an image with a large number of color variations, the average of the three RGB components converges to the same gray value K. In a physical sense, the gray-world hypothesis considers that the mean of the average reflection of light from a natural scene is a constant value on the whole, which is approximated as "grey".

Recent years have also witnessed the emergence of some deep learning-based LLIE methods that use the gray-world hypothesis as a loss function, and obtain impressive LLIE performance [8, 15, 16]. Where Zero-DCE [8] is the first to come up with the idea of formulating the gray-world hypothesis as a color constancy constraint as follows:

$$\mathcal{L}_{col} = \sqrt{\sum_{(p,q)\in S} (J^p - J^q)^2}, S = \{(R,G), (R,B), (G,B)\},\$$
(2)

where J^p and J^q represent the average values of the p and q channels in the enhanced image, respectively.

2.3. Mirror Visual Feedback Therapy

Mirror visual feedback (MVF) therapy was first introduced in early 1990s to relieve phantom limb pain in amputees. In the field of medicine, it is increasingly being used to treat several other chronic pain and functional rehabilitation of upper limbs in hemiplegic patients [21]. Fig.2 shows the principle of MVF therapy. During the treatment, the "affected side" of the hemiplegic patient is blocked by a flat mirror, while the patient can see the projection of the "healthy side" from the reflective surface of the mirror. As a result, when "rehabilitation training" is carried out on the "healthy side", due to the visual feedback, the patient will believe that the "affected side" is able-bodied, and indeed, the "affected side" is also miraculously getting better. It is worth noting that the patient's "affected side" doesn't perform any "rehabilitation training" during this process, but even so, the "affected side" can be treated better, which intuitively is a miraculous phenomenon.

3. Proposed Method

3.1. Motivation and Problem Statement

The current situation is that we need to enhance a low-light image via deep learning, but we have no LLIE task-related data for training, whatever type of data, including paired/unpaired/zero-reference data. In other words, we do not have a powerful paired constraint, an unpaired discriminative constraint, or even a gripper to use a non-reference constraint based on the zero-reference data. In such special case, how can we train a deep neural network to complete the task? Or do we really have hope to enhance a low-light image by deep learning without any task-related data?

A *simple effective* solution to this problem would probably have a major impact on the whole field of deep learning for computer vision (CV). Next, we mainly elaborate the potential impact of such a solution from two aspects.

For the LLIE task itself, this effective solution can avoid the inherent pitfalls of existing methods using task-related data, as described in Introduction. For all task-related data-based methods, the quality of the data determines the performance of the method. In other words, poor data quality leads to poor performance, which means that we need to collect good enough data, but the truth is that we have no idea what kind of data is so-called "good" for the proposed method. Thus, if this simple effective solution exists, the above pitfalls will no longer exist.

For the other CV tasks, this simple solution may allow for joint task processing in an elegant way. Recently, some works jointing LLIE with other tasks have emerged, e.g., joint with deraining [29], denoising [26], object/face

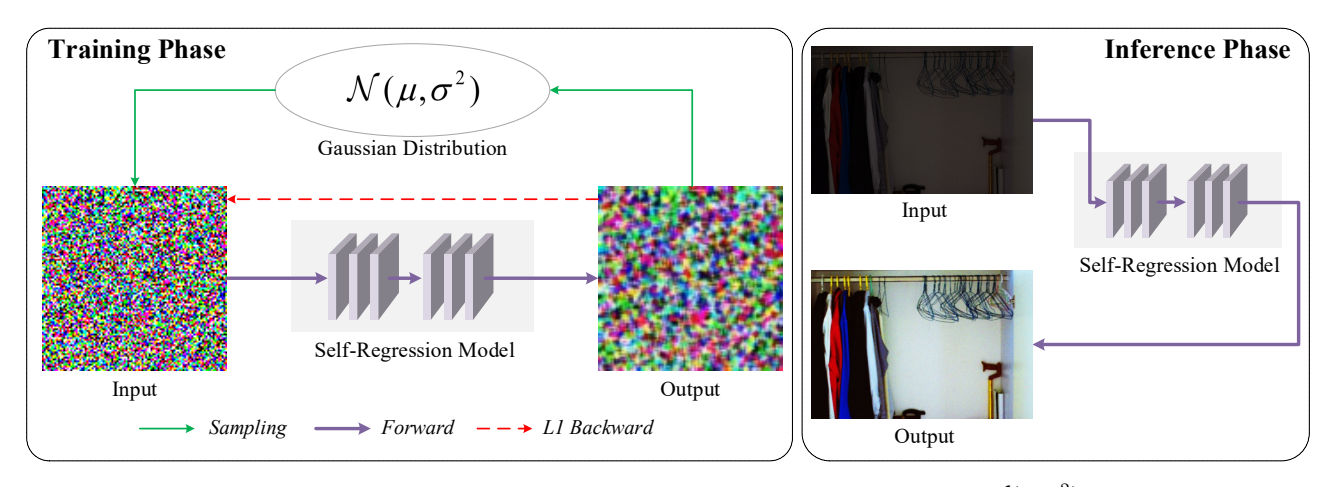


Figure 3. The training and inference pipeline of NoiSER. During training, just sampling $noise \sim \mathcal{N}(\mu, \sigma^2)$ iteratively to train a self-regression model (SRM). During inference, the trained SRM can directly enhance the low-light images and obtain impressive results.

detection [4, 17, 30, 31] or semantic segmentation [5]. The methods for all of these joint tasks tend to design a complex architecture to meet the task requirements. As such, if the solution discussed in this paper exists, considering the simplicity of which, there may be an elegant way to embed it into arbitrary CV task to achieve joint processing, since no LLIE-related data is needed to enhance an image.

3.2. Our Message

At first glance, solving such an enhancement problem seems impossible, since we don't have any available information to train a DNN. One conceivable solution for implementing deep training without task-related data is to borrow data from other similar tasks, which is exactly the idea of transfer learning [45]. For example, we can adopt the data from learning motorbikes to learn bicycles. However, this is not a real-sense solution, since the data are still needed to fine-tune the model finally. Is there really no way out?

In this paper, we will show that this problem not only can be solved, but also can be solved in an extremely elegant way. All what we need to solve this problem is just fully exploiting the three important theories in Section 2, i.e., image self-regression principle, gray-world hypothesis and mirror visual feedback therapy. We show that, based on the three theories, random noise can also exhibit great energy. A surprising message is that we will show that training a DNN by randomly sampling the noise can directly enhance a low-light image, which also perfectly solves the above problem. The following is the specific solution.

3.3. Solution?

3.3.1 Abstracting and meeting the task requirements

Let's recall the problem, i.e., "can we enhance low-light image based on deep learning without any task-related data?". We first decompose and abstract three requirements from

the problem: 1) any task-related data can't be used for training; 2) given an image, the output of the model should have similar content/texture to the input; 3) given a low-light image, the output of the model should be of normal light.

For the requirement (1), the easiest solution that comes to mind is to use the random noise to replace the task-related data. Thus, disregarding how to use the random noise, we at least have the determined data for training. The requirement (2) gives us a message that we need to train a model with a reconstruction capability. Considering the image self-regression principle, we can use the noise itself as supervisory signals to train the model. Now, we can meet the requirements (1) and (2) in a self-regression manner using random noise. For the requirement (3), we can force the output to satisfy the K-value gray-world hypothesis, where K should be in a normal gray range, such as 80-140 for the general 256 gray level.

Note that just meeting the above three requirements is still not enough to solve the problem, as there is one more important challenge, i.e., there is huge distribution gap between the training data (i.e., noise) and inference data (i.e., low-light images). Instead of narrowing the intractable distribution gap, the MVF therapy brings a fresh perspective, i.e., maybe we can roughly regard the forward propagation of non-task-related data as "healthy side", take the forward propagation of low-light images as "affected side", and see the self-regression as "rehabilitation training". Therefore, we no longer need to bother with the gap in distribution, but only need to adjust the self-regression training to find out what is really helpful in enhancing a low-light image. As a result, if we can eventually find a proper solution in the form of the MVF therapy, all we need to do is to clarify the mechanism behind the solution.

We show the ultimate pipeline of training and inference for an intuitive observation of our approach in Fig.3. It is noteworthy that noise itself is still relatively complex data.

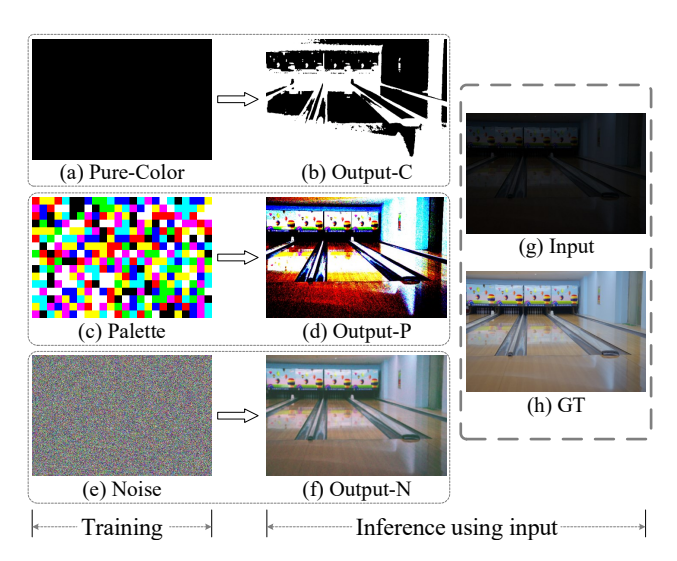


Figure 4. Comparison of fully-converged enhancement results using different training data. Clearly, the noise self-regression approach can yield visually better results.

Thus, prior to training with noise, we introduce two types of data with much simpler structures, i.e., pure-color (Fig.4(a)) and palette (Fig.4(c)). In what follows, we present and introduce three self-regressions asymptotically.

3.3.2 Pure-Color Self-Regression (C-Regression)

Considering the general 256 grey level, we first define the pure-color images (shortly, pure-color) as $I_c \in \mathbb{N}^{H \times W \times 3}$ under the following constraints:

$$\forall p_i, p_j \in I_c, \quad p_i = p_j$$

$$\forall p_i \in I_c, \quad max(p_i) \le 255,$$
(3)

where p_i, p_j denote pixels with three channels and $max(\cdot)$ denotes the maximum operation. Note that the "pure-" denotes an image rather than a color, e.g., pure-color image, pure-black image and pure-light-red image.

We first use pure-color for self-regression training due to two main reasons: 1) some low-light images themselves can be seen as pure-black with a degree of contrast, and 2) pure-color is very simple, which makes it easier to understand the effect of C-regression in enhancing low-light images, which is also instructive for the use of other more complex data.

Following the general image self-regression principle, as described in Eqn.1, C-regression is a process of minimizing the deviation between the model output and pure-color itself according to certain loss function:

$$\underset{\theta}{\arg\min} \, \mathbb{E}_{I_c} \{ L(f_{\theta}(I_c), I_c) \}, \tag{4}$$

where f_{θ} denotes a parametric family of mappings and L_1 loss is used for optimization. Please kindly note that we use the fixed pure-color for C-regression training.

We first use pure-black for training and directly use the trained model to enhance a low-light image, as shown in

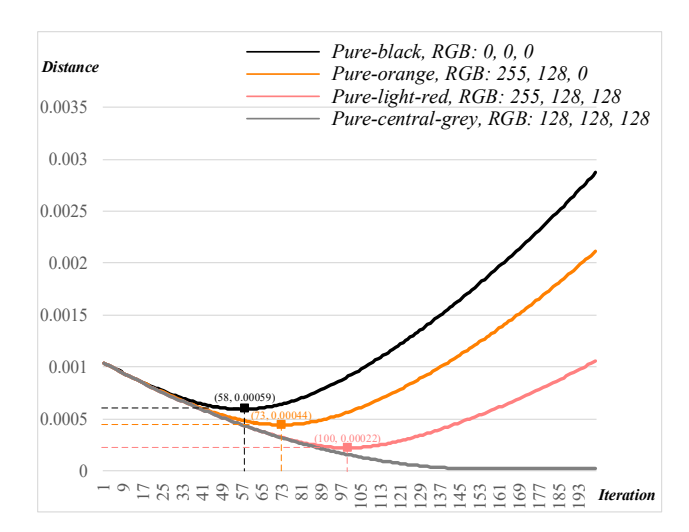


Figure 5. Iteration-Distance curves using different pure-colors for C-regression training. The distance is the L_2 norm between the output and the pure-central-grey during training.

Fig.4(g) and Fig.4(b). We can easily see that the low-light input is crudely broken down into binary colors, i.e., black and white, which implies that pure-black can't enhance image although it is close the dark images. However, we still got some inspiration, e.g., C-regression has roughly reconstructed the texture of the input. Thus, it is crucial to reveal the mechanism of how the input is divided into two colors.

Deep neural networks often work in black box manner and we cannot explain the intrinsic mechanism at the micro level. But at the macro level, we can still obtain a correct conclusion based on induction reasoning. Specifically, we follow the steps of incomplete induction reasoning, i.e., individual phenomenon \rightarrow individual conclusion \rightarrow universal $conclusion \rightarrow intra-domain\ validation$. Specifically, based on the phenomenon of pure-black self-regression (i.e., dividing low-light input into black and white), we can induce an individual conclusion and then generalize it from individual to universal, and as a result, this universal conclusion can be applied to other pure-color (e.g., pure-red). Then, we need to perform self-regression training experiments using other colors, and if the experimental results also satisfy the universal conclusion, this conclusion can be proven to be correct. Prior to perform incomplete induction reasoning, we introduce the required definitions and propositions.

Definition 1 (central grey): For a specific range of image values [a,b], the central grey is a color $C_g \in \mathbb{R}^3$ if it satisfies

$$C_g^i = \frac{a+b}{2}, \quad i \in \{R, G, B\},$$
 (5)

where $C_g=(127.5,127.5,127.5)$ in the general 256 grey level (range: [0, 255]), while actually the channel value is replaced by 128, since only integers are allowed.

Definition 2 (opposite color): For a specific range of image values [a,b], a color $C_1 \in \mathbb{R}^3$ is the opposite color of

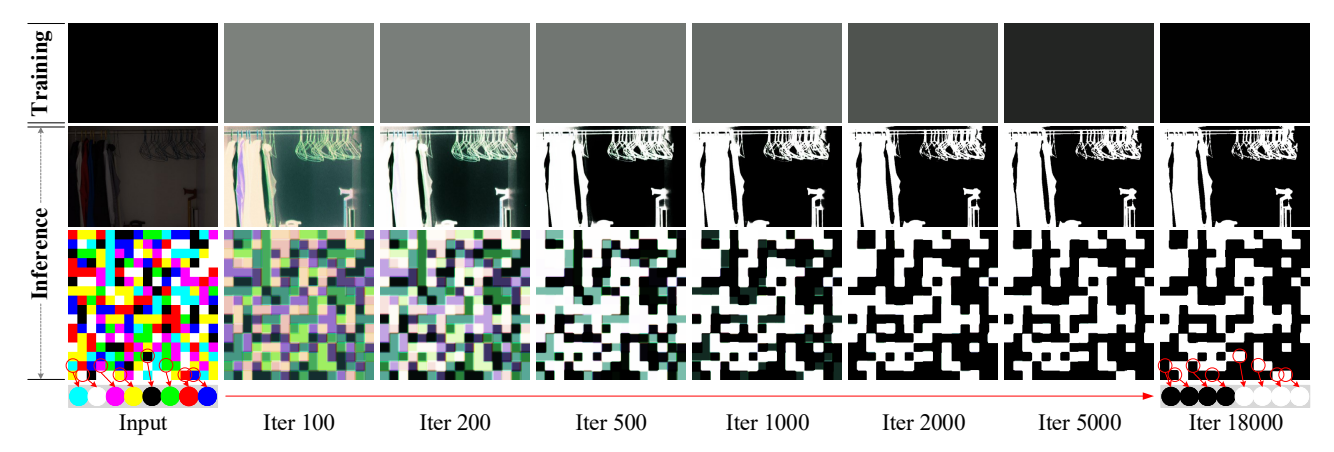


Figure 6. The phenomenon obtained from the pure-black self-regression. For an arbitrary input with a degree of contrast, the model finally tend to divide the input to be either black or white.

the color $C_2 \in \mathbb{R}^3$ if they satisfy the following condition:

$$|C_1^i - C_a^i| = |C_2^i - C_a^i|, \quad i \in \{R, G, B\},$$
 (6)

where C_g denotes the central grey, and $C_1 \neq C_2$.

Proposition 1: Based on a model with random initialization, arbitrary C-regression tends to construct the purecentral-grey in the initial iterations.

Validation for Proposition 1: Given an image I, we use Eqn.2 to measure the distance between this image and the pure-central-grey with small modification as follows:

$$\mathcal{D}(I) = \sqrt{\sum_{i \in S} (I^i - C_g^i)^2}, \quad S = \{R, G, B\}, \quad (7)$$

where I^i is the average value of the i channel in image I.

In this study, we choose four pure-colors with different distances from the pure-central-grey for validation, i.e., pure-black (RGB(0,0,0)), pure-orange (RGB(255,128,0)), pure-light-red (RGB(255,128,128)) and the pure-central-grey itself (RGB(128,128,128)). Clearly, the relation of the distances satisfies: $\mathcal{D}(\text{pure-black}) > \mathcal{D}(\text{pure-orange}) > \mathcal{D}(\text{pure-light-red}) > \mathcal{D}(\text{pure-central-grey}) = 0$. In Fig.5, we show the iteration-distance curves based on these pure-colors during C-regression training. For non-pure-grey self-regression training, no supervised signals are pure-grey; nevertheless, the overall trend of the curves is initially down and then up rather than directly up, which indicates Proposition 1 is True. For the pure-grey self-regression training, the curve falls directly and converges gradually, which additionally proves the correctness of Proposition 1.

Individual phenomenon. Fig.4(a), Fig.4(g) and Fig.4(b) show an example of using pure-black self-regression training to infer a low-light image. We see from Fig.4(h) and Fig.4(b) that the trained model tends to map some colors (e.g., white and yellow) to the color used in C-regression training (i.e., black, RGB(0,0,0)), while mapping the other colors (e.g., black, red and green) to the opposite color (i.e.,

white, RGB(255,255,255)). This inspires us to explore the mapping relationship of the colors before and after inference. To this end, we build a palette containing rich colors as the image to be inferred. Fig.6 shows the process of inferring a low-light image and shows a palette in pure-black self-regression iterative training. We see that there are 8 colors in the palette, of which 4 colors (i.e., cyan, white, purple and yellow) are mapped to black and the other 4 colors (i.e., black, green, red and blue) are mapped to the opposite color of black, which is applicable to each pixel in the palette.

Individual conclusion. Table 1(a) illustrates the specific induction process from individual phenomenon to individual conclusion based on pure-black self-regression. Specifically, the individual phenomenon is shown in rows 4 and 12, while the induction process of the individual conclusion is shown in rows 1-3 and 5-11. During training, Proposition 1 tells us that the initial output tends to the pure-central-grey (row 1); as the iterations increase, the output becomes very close to the pure-black (row 2). Thus, we can find that for all three RGB channels, the pure-black self-regression perhaps learns a downtrend (row 3). During inference, we see from the phenomenon that the input is divided into black and white (rows 4 and 12), which may be related to the learned trends. To this end, firstly, we list the RGB values (rows 5-7) of the colors in the fourth row; secondly, we check whether the specific channel satisfies the learned trend (rows 8-10). Taking "Cyan" as an example, since all three RGB channels learn to trend down, the G,B channels in "Cyan" satisfies the trend, but R channel does not (0 will overflow if a downward trend is taken); thirdly, we record the number of channels that satisfy the learned trend (row 11); finally, based on the results in row 11 and the observations in row 12, we believe if a color meets at least two channel trends, it will be mapped to black (i.e., training color), and conversely, to white (the opposite of training color).

Universal conclusion. According to the individual con-

			\sim	C .1		1	DD 11	
ism.	mechan	-regression	C	of the	ı C	lustration	Table	
. 1	mccman	10210331011	_	<i>n</i> uic		iusuanon	1 aut	

	(a) Individual phenomenon \rightarrow Individual conclusion								(b) Universal conclusion $ o$ Intra-domain validation												
Training (Black)	1	Initial R:128 G:128 B:128				Training	nining 1 Initial R:128 G:128 B:128														
	2	Final	R:0	G:0	B:0		Black or White /			(Red)	Y Pinal R: / 22 G:U B:U Red Or C					or Cya	yan?				
	3	Trend	R:↓	G:↓	В:↓					(Keu)	3	Trend	R:↑	G:↓	В:↓						
	4	Color	White	Cyan	Purple	Yellow	Red	Green	Blue	Black		4	Color	White	Cyan	Purple	Yellow	Red	Green	Blue	Black
	5	R↓	255	0	255	255	255	0	0	0		5	R↑	255	0	255	255	255	0	0	0
	6	G↓	255	255	0	255	0	255	0	0	Inference	6	G↓	255	255	0	255	0	255	0	0
	7	B↓	255	255	255	0	0	0	255	0		7	B↓	255	255	255	0	0	0	255	0
Inference	8	R?	✓		\checkmark	\checkmark	\checkmark					8	R?		\checkmark				\checkmark	\checkmark	\checkmark
	9	G?	✓	\checkmark		\checkmark		\checkmark				9	G?	✓	\checkmark		\checkmark		\checkmark		
	10	В?	✓	\checkmark	\checkmark				\checkmark			10	В?	✓	\checkmark	\checkmark				\checkmark	
	11	No.	3	2	2	2	1	1	1	0		11	No.	2	3	1	1	0	2	2	1
	12	То	Black	Black	Black	Black	White	White	White	White		12	То	Red?	Red?	Cyan?	Cyan?	Cyan?	Red?	Red?	Cyan?

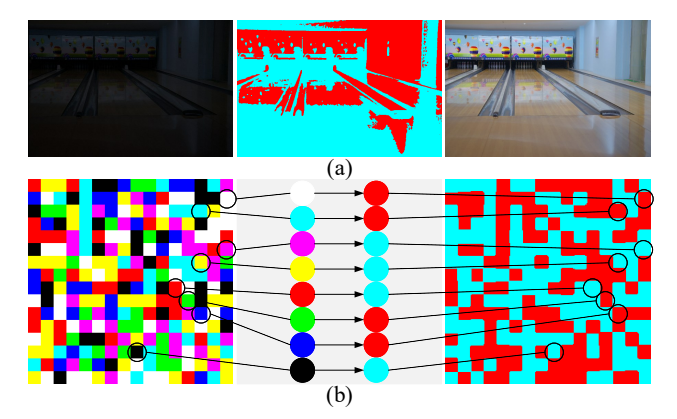


Figure 7. Intra-domain validation using pure-red self-regression.

clusion, we can directly generalize it to a universal one, i.e., during training, C-regression attempts to learn the trends of the three channels of RGB. During inference, if a color satisfies over two channel trends, it will be mapped to the training color, otherwise, to the opposite of training color.

Intra-domain validation. To verify the correctness of the universal conclusion, we need to perform C-regression training based on the other colors and see whether the experimental results are consistent with this conclusion. Taking the pure-red self-regression as an example, we perform the reasoning process in Table 1(b). Row 12 displays the reasoning results, from which we see that white, cyan, green and blue are mapped to red, while purple, yellow, red and black are mapped to cyan. We further conduct and display the corresponding experiments in Fig.7. Clearly, the results keep consistent with the reasoning results, which proves that the conclusion is correct. More experimental results can be found in the supplementary material. Here, there is one point that must be noticed, i.e., the condition for the above conclusion to be valid is that the distribution between the training and inference data is far different.

At this point, we have fully understood the mechanism of C-regression and can assert the following facts:

• C-regression initially implements the reconstruction of the input texture, and if the texture integrity is not considered for the LLIE task, C-Regression already satisfies the requirements (1) and (2) in Section 3.3.1. The color binarisation of the C-regression results relies on the color homogeneity in the training samples, and it is conceivable that a more accurate texture might be reconstructed if each training sample is enriched with multiple colors and has a degree of contrast.

3.3.3 Palette Self-Regression (P-Regression)

In Section 3.3.2, we have used the palette for inference, and here we will illustrate that using the palette as training data for self-regression allows for a generation of normal-light image and a finer reconstruction of the image textures. Considering the general 256 grey level, we can define the palette as $I_p \in \mathbb{N}^{H \times W \times 3}$ with the following constraints:

$$\forall q_i, q_j \in I_p, \quad grain(q_i) = grain(q_j)$$

$$\forall q_i \in I_p, \ \forall p_i, p_j \in q_i, \quad p_i = p_j$$

$$\forall q_i \in I_p, \ \forall p_i \in q_i, \quad max(p_i) \le 255,$$

$$(8)$$

where q_i,q_j denote non-overlapping patches, $grain(\cdot)$ denotes the grain of the patch (setting grain size to 16 in this work), p_i,p_j denote pixels with three channels and $max(\cdot)$ denotes the maximum operation. From the above definition, the palette can be regarded as the coarse-grained noise and as the fine-grained pure-color. We provide the pseudo-code for building the palette in the supplementary material.

Similar to C-regression, given palettes as training data, P-regression is the process whereby the palette learns to rebuild itself according to certain loss function:

$$\arg\min_{\theta} \mathbb{E}_{I_p} \{ L(f_{\theta}(I_p), I_p) \}, \tag{9}$$

where f_{θ} denotes the parametric family of mappings, and we also use the L_1 loss for optimization.

Fig.4(g) and Fig.4(d) show an example of inferring a low-light image through P-regression. As can be seen, P-regression successfully reconstructs the texture of the given low-light image. Next, we first introduce a required propositions to seek the mechanism behind P-regression.

Proposition 2: Based on a model with random initialization, P-regression tends to start building the pure-central-grey at a starting point and continues until converges.

Table 2. List of RGB channel means for different datasets under the general 256 grey level. We can conclude that, for an image of normal light, the RGB channel means often fall in the range of 80-140. In addition, we also find that the RGB channel means are smaller for overdark images and larger for overexposed images.

	LOI	L [33]		LSRW	SCIE [2]				
Sets	LOL	LOL	LSRW (Huawei) LSRW (Huawei) LOL		LOL (Nikon)	LSRW (Nikon)	SCIE	SCIE	SCIE
	-Normal	-Overdark	-Normal	-Overdark	-Normal	-Overdark	-Normal	-Overdark	-Overexposed
R	120.47	15.49	110.39	18.92	122.69	42.26	122.12	32.78	164.82
G	113.88	15.22	98.22	16.39	124.55	43.19	121.18	32.71	161.40
В	110.38	14.73	86.63	15.20	124.69	43.48	109.77	31.07	149.51

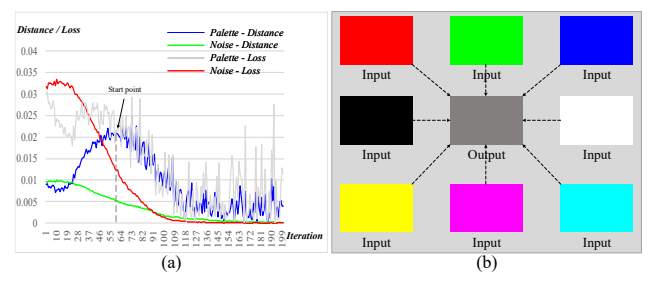


Figure 8. (a) Iteration-Distance/Loss curves for P-regression and NoiSER training. The distance is L_2 norm between output and pure-central-grey during training, and the loss is color constancy loss of output. (b) Pure-color mappings after training.

Validation for Proposition 2: Given an image I, similar to C-regression, we use Eqn. 7 to measure the distance between this image and the pure-central-grey. The blue curve in Fig. 8(a) shows the distance between the output and pure-central-grey. We see that after a certain starting point (about 61st iteration), the output gradually approaches the pure-central-grey, although we did not add any constraints to this during the training process, which means that Proposition 2 is True. Besides, we use pure-colors as inference images for validation, and obtain a consistent conclusion with Proposition 2, i.e., all outputs appear grey (see Fig. 8(b)).

Proposition 3: Known ①: The image satisfies the K-value gray-world hypothesis, where K is approximately between 80 and 140; Known ②: The image is of normal light. Then, ① is a statistically necessary condition for ②.

Validation for Proposition 3: Table 2 shows the RGB channel means (i.e., the mean value of each color channel) for several widely-used-datasets, including two real-world datasets (LOL [33] and LSRW [10]) and a multi-exposure dataset (SCIE [2]). We conclude that: (1) all datasets satisfy gray-world hypothesis (the channel deviation is also not too large for LSRW (Huawei)-Normal); (2) the channel means of the normal datasets usually lies between 80-140. Note that (1) and (2) provide the proof of *Proposition 3*.

For P-regression, the training samples themselves have a degree of contrast (variation between non-overlapping patches), which ensures that P-regression can reconstruct the texture of image more accurately than C-regression. In addition, according to *Propositions 2* and 3, we know that the P-regression has the ability of mapping any color to ap-

proach grey, which means that the channel means of the output meet the K range (80-140) of the normal-light images. As a result, suppose that the P-regression further satisfies the gray-world hypothesis, we can use P-regression to get the normal-light output that satisfies all three requirements mentioned in Section 3.3.1. However, this supposition is valid but not strictly. We use the color constancy loss (Eqn.2) to measure the satisfaction degree towards the grayworld hypothesis (not applying it to back propagation). As the grey curves in Fig.8(a) show, the overall downward trend suffers from sharp fluctuations. Nevertheless, the P-regression can still yield a relatively favorable result.

Now, we can clarify the mechanism of P-regression and can assert the following facts:

- P-regression initially meets all the three requirements mentioned above, which means that P-regression can already enhance a low-light image properly.
- The enhancement results of P-regression are unpleasant due to the sharp fluctuations in the convergence to gray-world hypothesis. It is conceivable that a more pleasing result might be generated, if we can smooth out the sharp curve fluctuations.

3.3.4 Noise Self-Regression (NoiSER)

Considering that one possible reason for sharp curve fluctuations is the larger grain size of the patches in a palette, we attempt to use noise for self-regression training, since noise can be approximated as a fine-grained palette.

Instead of defining an additional noise, we directly sample a Gaussian noise $I_n \sim \mathcal{N}(\mu, \sigma^2)$, and the specific regression process can be expressed as follows:

$$\underset{\theta}{\arg\min} \, \mathbb{E}_{I_n} \{ L(f_{\theta}(I_n), I_n) \}, \tag{10}$$

where f_{θ} denotes the parametric family of mappings. Similar to both C-regression and P-regression, we still use the L_1 loss for optimization.

Fig.4(g) and Fig.4(f) show an example of inferring a low-light image via NoiSER. As can be seen, given a low-light input, NoiSER successfully generates a visually pleasing enhanced result. We first introduce a required proposition to understand the specific mechanisms of NoiSER.

Table 3. Numerical results on the LOL dataset [33], where the best performance is marked in red and the second best one is marked in
blue. Clearly, our NoiSER has significant advantages, not only for performance metrics but also for application metrics.

-	Training data	Methods	Perfor	mance m	etrics	Application metrics			
	Training data	Methods	PSNR↑	SSIM↑	NIQE↓	$TT\downarrow(min)$	$\text{IT}\downarrow(ms)$	No.P↓	
Optimization		LIME [9]	14.2216	0.5144	8.5828	-	104553.82	-	
-based	-	Zhang et al. [37]	14.0181	0.5130	8.6111	-	138127.48	-	
	Paired	RetinexNet [33]	16.7740	0.4191	9.7294	3.17	95.40	1,333,841	
	Unpaired	EnlightenGAN [12]	18.5413	0.6880	5.7111	90.05	10.91	6,959,553	
	Zero-reference	Zero-DCE [8]	14.9672	0.5003	8.4228	16.33	2.24	79,416	
Deep learning		Zero-DCE++ [15]	14.8039	0.5161	8.3412	24.12	1.51	10,561	
-based		RUAS [18]	16.4047	0.4996	5.9297	-	8.57	3,438	
-baseu		SCI [20]	14.0226	0.5080	8.3315	2563.68	1.12	258	
		NoiSER-FC (Ours)	17.5748	0.7134	3.7285	1.10	1.21	1,323	
	Task-irrelevant	NoiSER-ES (Ours)	17.0250	0.6563	3.7206	0.58	1.21	1,323	
		NoiSER-Var3 (Ours)	14.9257	0.5998	3.6806	1.10	1.21	1,323	

Table 4. Comparison of generalization performance on the LSRW dataset [10], where the best performance is marked in red and the second best one is marked in blue. Clearly, our NoiSER has a stronger generalization ability over different datasets than all other methods.

	Training data	Methods	LSF	RW (Huaw	/ei)	LSRW (Nikon)			
	Training data	Wiethous	PSNR↑	SSIM↑	NIQE↓	PSNR↑	SSIM↑	NIQE↓	
Optimization		LIME [9]	15.3376	0.4360	3.0148	14.6362	0.3777	3.3818	
-based	-	Zhang et al. [37]	14.0984	0.4327	2.9228	13.0886	0.3677	3.4620	
	Paired	RetinexNet [33]	16.8127	0.3948	4.3349	13.4853	0.2934	4.2774	
	Unpaired	EnlightenGAN [12]	16.8448	0.4832	3.0916	14.9071	0.4065	3.3745	
	Zero-reference	Zero-DCE [8]	14.2002	0.3958	3.5864	11.8197	0.3550	3.9127	
Deep learning		Zero-DCE++ [15]	14.2370	0.4163	3.4862	11.0893	0.3675	3.7375	
-based		RUAS [18]	15.6867	0.4909	3.0399	12.1426	0.4372	3.9902	
-based		SCI [20]	15.2583	0.4233	3.1263	14.4512	0.4092	3.7864	
		NoiSER-FC (Ours)	15.7268	0.5407	3.3555	15.5537	0.4657	3.7784	
	Task-irrelevant	NoiSER-ES (Ours)	15.6968	0.5264	3.0696	15.7090	0.4584	3.4976	
		NoiSER-Var3 (Ours)	15.3001	0.5193	2.9714	15.5260	0.4672	3.5445	

Proposition 4: Based on a model with random initialization, NoiSER tends to learn a gray-world mapping, i.e., learning to approach pure-central-grey while satisfying the gray-world hypothesis.

Validation for Proposition 4: Given an image *I*, similar to P-regression, we use Eqn.7 to measure the distance between *I* and the pure-central-grey, and use Eqn.2 to measure the satisfaction degree towards the gray-world hypothesis. The green and red curves in Fig.8(a) demonstrate the specific iterative processes. As can be seen, although we do not apply the equation for back propagation, the curves will still converge smoothly, which demonstrate the correctness of *Proposition 4*. Similar to P-regression, NoiSER training can also make pure-colors appear grey (see Fig.8(b)).

Thus, it's clear that NoiSER satisfies all the properties of P-regression while smoothing the convergence curve towards the gray-world hypothesis, which makes it possible to generate the pleasing LLIE results. In a word, our proposed NoiSER approach aims at learning a gray-world map-

ping during training, and the learned mapping can enhance a low-light image during inference. Finally, we demonstrate the pipelines for NoiSER training and inference, as shown in Fig.2. The specific structure of the self-regression model (SRM) is detailed in the supplementary material.

4. Experimental Results and Analysis

4.1. Experimental Descriptions

Method description. Training our NoiSER to full convergence (denoted as NoiSER-FC) will yield a better quantitative performance, however we observe that the visual effect appears to be obscured by a gray layer since NoiSER aims at learning a gray-world mapping. As such, we use an early stopping mechanism (denoted as NoiSER-ES), trading part of the quantitative performance for visual improvement. In addition, to obtain better visual effect, we improve the contrast between noisy neighboring pixels by raising the variance of the standard Gaussian distribution to 3 (denoted NoiSER-Var3). We will conduct extensive experiments to



Noise self-regression

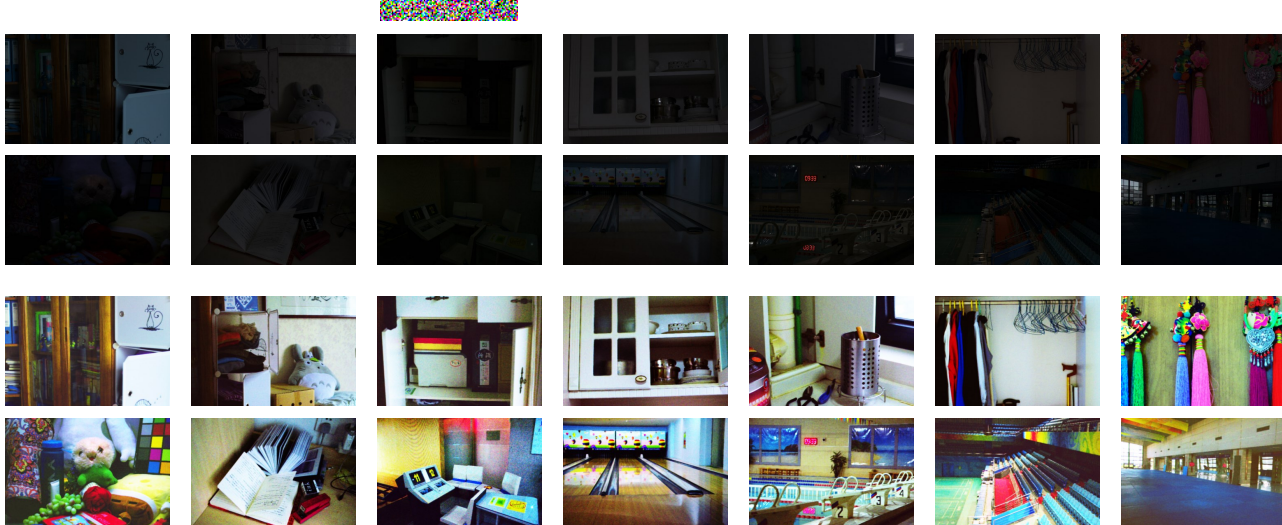


Figure 9. Intuitive visual display of our NoiSER on most widely-used LOL dataset. We manually exclude "23.png" due to its similarity to "22.png", facilitating a two-line display. Just a simple and straightforward noise self-regression can yield a surprising visual effect.

show the results of the three variants of NoiSER. Due to the special nature of NoiSER, a few hiccups are inevitable. But these hiccups are obviously trivial, since the training of our NoiSER is extremely fast, taking only about 1 minute.

Comparison description. Since our NoiSER does not use any task-related data for training, all the tests on different datasets are equivalent to evaluating the generalization ability of NoiSER, instead of the fitting ability. Training and testing on the same dataset is apparently against our intent, however we still use the most widely-used LOL dataset [33] (training & testing) to show that our method is competitive.

4.2. Experimental Settings

Evaluated datasets. We first conduct experiments on two real-world image datasets: LOL [33] and LSRW [10]. LOL is used to measure the fitting capability of other compared methods by training and testing on it, and LSRW is used to measure the generalization capability of all compared methods by directly testing on it using the pretrained model on LOL dataset. Besides, we use a multi-exposure dataset (SCIE [2]) to measure the overexposure suppression capability of each method. The details are as follows:

- LOL: LOL is the most widely-used dataset for LLIE task, including 485 training pairs and 15 testing pairs with resolution 400×600.
- LSRW: LSRW includes two subsets: LSRW (Huawei) and LSRW (Nikon). LSRW (Huawei) has 2,480 training pairs and 30 testing pairs with resolution 720×960,

- while LSRW (Nikon) contains 3,170 training pairs and 20 testing pairs with resolution 640×960 .
- SCIE: SCIE includes 4,413 multi-exposure images with resolution between 3000×2000 and 6000×4000. It is divided into two parts, namely, "Dataset_Part1" and "Dataset_Part2", and we only adopt the overexposed image named "7.JPG" from "Dataset_Part2" as an example in our experiments.

Evaluated metrics. We use three widely-used metrics to evaluate the quantitative performance of each method, including two full-reference metrics (i.e., peak signal-to-noise ratio (PSNR) and structural similarity (SSIM) [32]) and one no-reference metric (i.e., naturalness image quality evaluator (NIQE) [22]). Besides, we also use three *application* metrics to evaluate the possibility of each method for practical deployment and application, i.e., training time (TT), inference time (IT) and number of parameters (No.P). In all experiments, we use the ↑ to indicate the higher the better, and use the ↓ to indicate the lower the better.

Compared methods. Two optimization-based methods (LIME [9] and Zhang et al. [37]) and six deep learning-based methods are included for comparison. For those deep models, different types of training data are leveraged to fit the model, i.e., paired (RetinexNet [33]), unpaired data (EnlightenGAN [12]) and zero-reference data (Zero-DCE [8], Zero-DCE++ [15], RUAS [18] and SCI [20]). Note that we mainly compare with the four zero-reference methods, as they are closer to our NoiSER in terms of data constraints.

Implementation details. Based on PyTorch 1.10.1 [24]

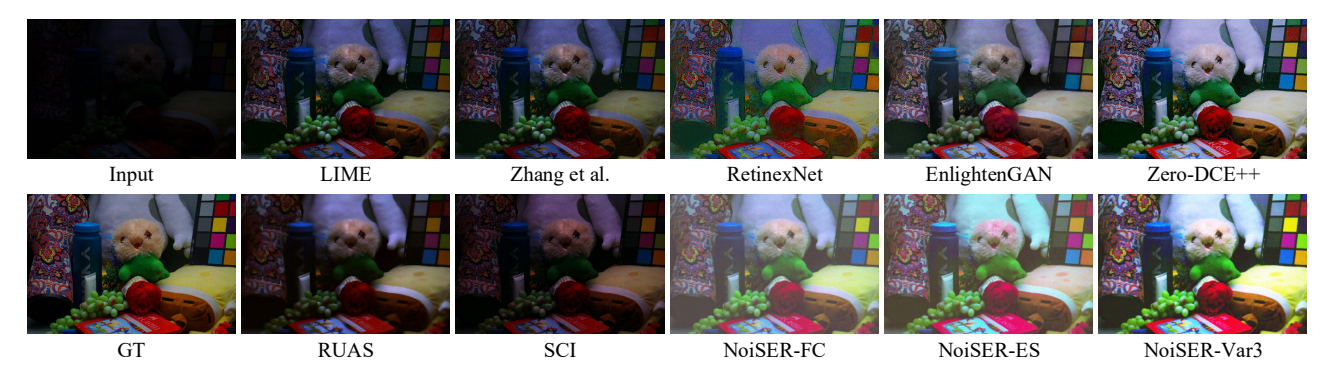


Figure 10. Visual results of different enhancement methods base on the LOL dataset [33], including LIME [9], Zhang et al. [37], RetinexNet [33], EnlightenGAN [12], Zero-DCE++ [15], RUAS [18], SCI [20] and our NoiSER. Clearly, our NoiSER obtains better visualization effects, despite no task-related data has been used for training. Specifically, our NoiSER can enhance the image contents more visibly and naturally, even beyond the ground-truth, which is attributed to the ability of our method to learn a gray-world mapping.

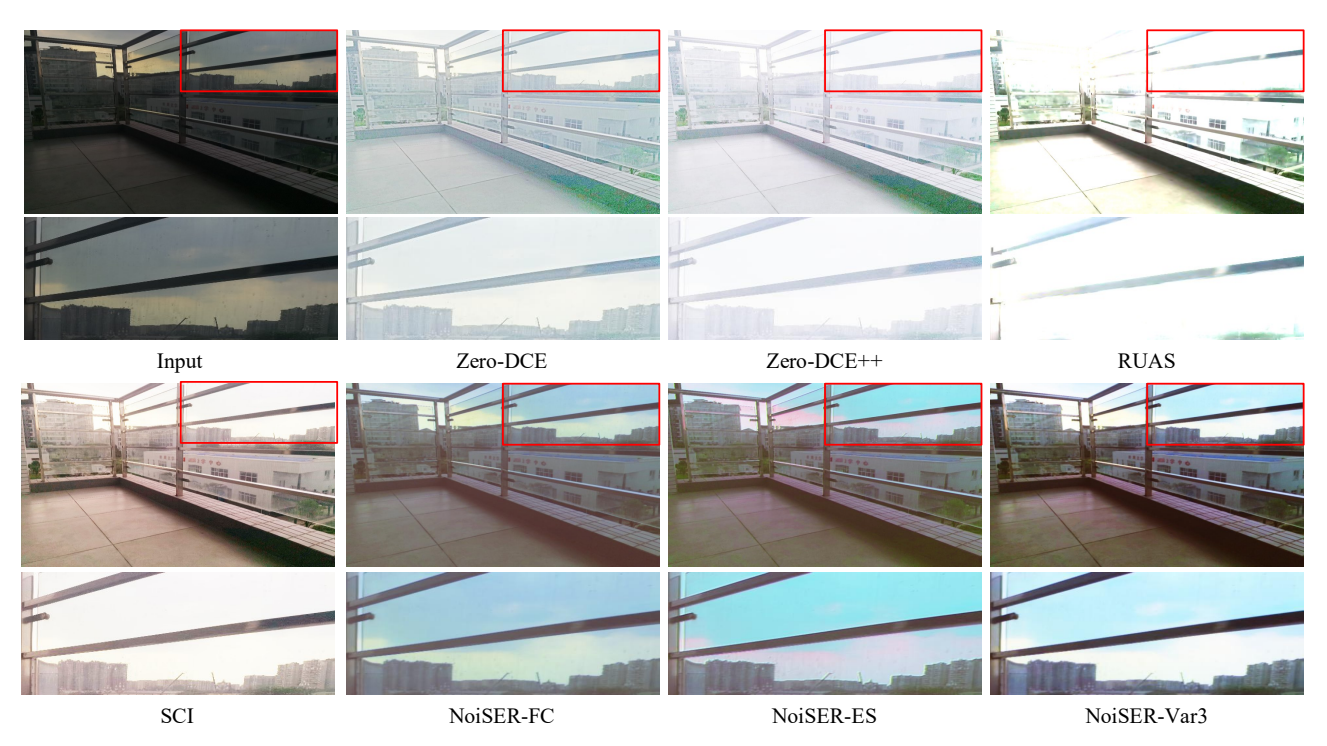


Figure 11. Visual results of different enhancement methods based on the LSRW (Huawei) dataset [10], including Zero-DCE [8], Zero-DCE++ [15], RUAS [18], SCI [20] and our NoiSER. For each method, the top row shows the original enhanced images and the bottom row shows the zooming in of the enlarged detail ine red boxes. Clearly, all other compared methods overexpose the brighter areas of the image, while our NoiSER effectively suppresse the exposure and does a good job in recovering the texture detail of the image.

and Python 3.6.9, we train and evaluate our NoiSER on single NVIDIA RTX 2080 Ti GPU. We train our NoiSER for 2000 iterations (600 for NoiSER-ES) with a batch size of 1 and a fixed learning rate of 2e-4. We sample the noise from standard Gaussian distribution $\mathcal{N}(0,1)$ ($\mathcal{N}(0,3)$) for NoiSER-Var3) with a shape of 104×104 for training. Besides, the Adam optimizer [13] is utilized for training with $\beta_1 = 0.5$ and $\beta_2 = 0.999$. To alleviate the noise in the enhanced results, we add TV regularization during training.

The total loss function of NoiSER is defined as

$$\mathcal{L}_{total} = \mathcal{L}_{l_1} + \mathcal{L}_{tv}. \tag{11}$$

4.3. Quantitative Evaluations

4.3.1 Results on LOL dataset

To examine the fitting ability of each method, we first evaluate each model on LOL, in terms of three performance metrics (PSNR, SSIM and NIQE) and three application metrics

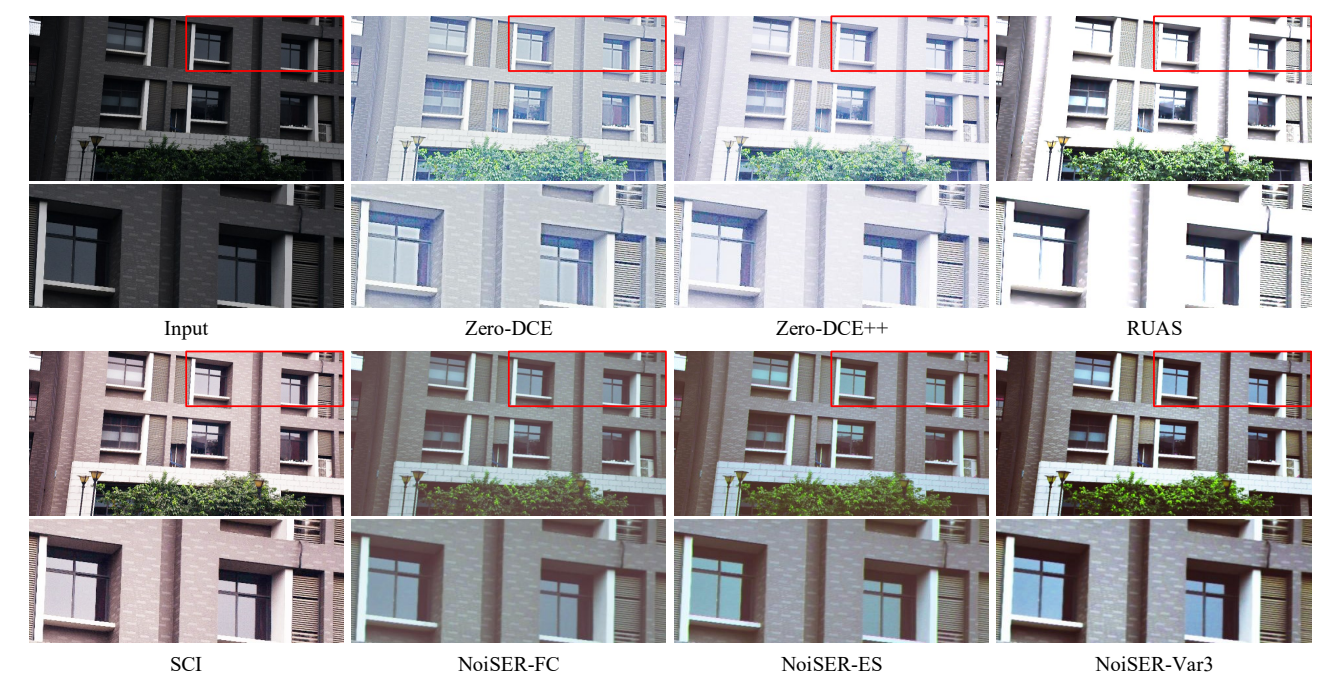


Figure 12. Visual results of different enhancement methods based on the LSRW (Nikon) dataset [10], including Zero-DCE [8], Zero-DCE++ [15], RUAS [18], SCI [20] and our NoiSER. Because the image itself is not very dark, all other compared methods either overexpose the image or distort the color, while our NoiSER achieves a better visual result.

(TT in minutes, IT in milliseconds and No.P). The numerical results are shown in Table 1. We did not list the training time of RUAS [18], since it involves a process of neural architecture search. For the TT metric, we get the result on a single NVIDIA RTX 2080 Ti using the default configuration according to the codes provided by authors. We can find that: 1) the optimization-based methods take longer inference time for the use of CPU for computation, which will be a major impediment to real applications; 2) when training with paired/unpaired data, RetinexNet and Enlighten-GAN yield better performance due to the relatively strong constraints, however, they have a larger number of parameters and slower inference speed; 3) the zero-reference methods require minimal computational resources, which are relatively efficient and have a stronger application potential; 4) although our NoiSER does not use any task-related data for training, it is still highly competitive to the other methods across all metrics. From the comparison to the zeroreference methods, our NoiSER perfectly outperforms all of them, with significantly less training time.

4.3.2 Results on LSRW dataset

To measure the generalization ability, we evaluate the methods on two test subsets, i.e., LSRW (Huawei) and LSRW (Nikon). The numerical results are shown in Table 2. We can find that: 1) the models fitted using task-related data fail to generalize well to all datasets, since they perform well on some datasets but poorly on others. For example, Enlight-

enGAN [12] and RetinexNet [33] obtains the best records on LSRW (Huawei), but worse on LSRW (Nikon), which is inevitable for the usage of task-related data; 2) our NoiSER generalizes generally well and is more balanced¹ across different datasets, indicating that our approach is closer to the essence of low-light enhancement; 3) from the comparison to those zero-reference methods that are more close to ours, our NoiSER obtains significant superiority in all metrics.

4.4. Visualization Evaluations

4.4.1 Visual Analysis on LOL Dataset

NoiSER is easy to implement and yields surprising results. Considering that the test set of LOL only has 15 low-light images, we show the entire set to give a more intuitive view for the enhancement effect in Fig.9. By simply performing a noise self-regression for training, all low-light images can be enhanced with rich texture, content and color.

We then compare each method on a extremely dark image (from which human eyes hardly see anything) of LOL [33] dataset in Fig.10 . We see that: 1) both optimization-based methods and deep learning models using task-related data can enhance this very dark image to some extent, but the restored images are still inferior, in terms of illumination enhancement, detail recovery and color preservation; 2) our NoiSER enhances this overdark image considerably, and

 $^{^{\}rm I}$ It means that NoiSER generalizes stably on different datasets, i.e., it is less likely to be extremely good on one, but extremely poor on the other.

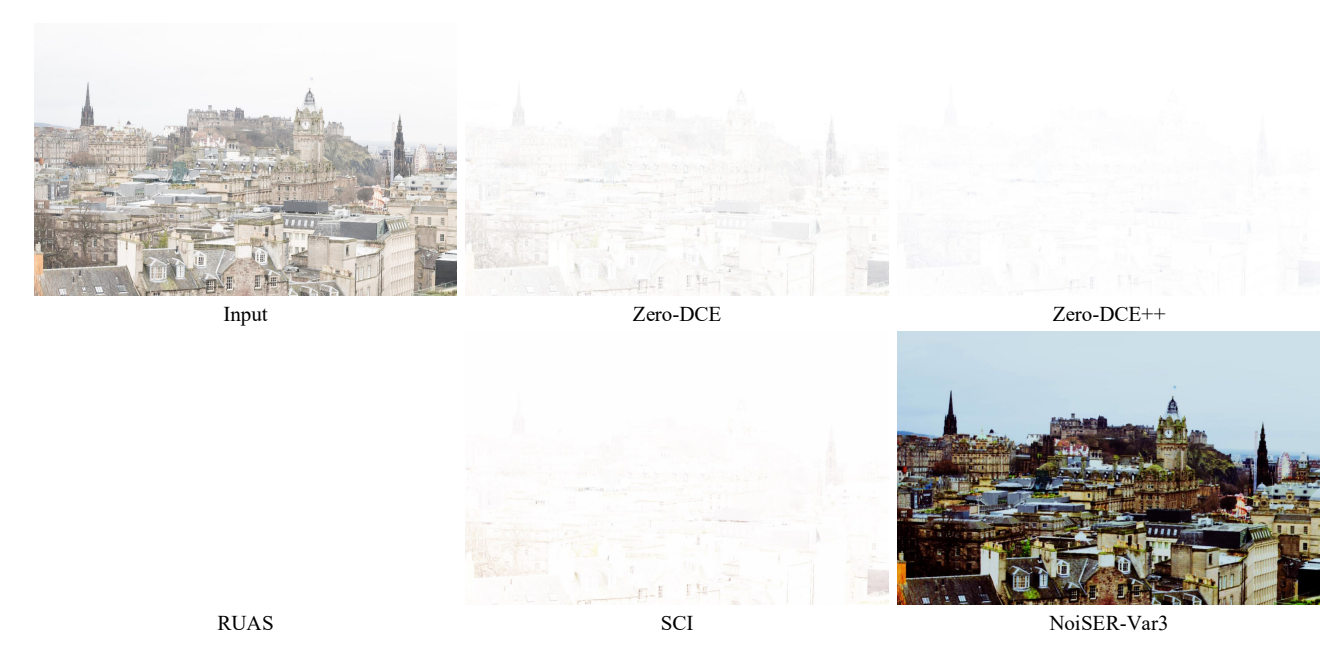


Figure 13. Comparison of the overexposure suppression effects of each method on the SCIE dataset [2], inclduing Zero-DCE [8], Zero-DCE++ [15], RUAS [18], SCI [20] and our NoiSER. We see that all other competitors failed to handle the overexposed inputs appropriately, while our NoiSER has an inborn automated exposure suppression capability.

the restored image is even beyond the brightness and content naturalness of the ground-truth, which can be attributed to the learned gray-world mapping that always forces the channel means of a low-light image to be close to the central grey; 3) for the visual effects of several variants of our NoiSER, NoiSER-FC < NoiSER-ES < NoiSER-Var3. As mentioned in Section 4.1, NoiSER-FC seems to be covered by a grey layer, which should be caused by the learned gray-world mapping, and NoiSER-ES shows that early stopping mechanism can alleviate this issue. To obtain the most visually pleasing effect, we can adopt the manner of increasing the variance of Gaussian distribution, since NoiSER-Var3 clearly shows a better visual effect.

4.4.2 Visual Analysis on LSRW Dataset

To evaluate the generalization ability by visual analysis, we compare the visual results of each method on LSRW [10] dataset in Figs.11 and 12. We see that: 1) when input image is not very dark, zero-reference methods tend to produce overexposure enhanced images. One possible solution to this issue is to train the model with a relatively large multi-exposure dataset, implying that appropriate training data must be picked as carefully as possible. Despite this, it is still tricky to determine which datum is so-called appropriate to handle the complex distribution of low-light images in reality; 2) owing to the simple and straightforward training process, our NoiSER has a powerful generalization power. From the comparison of the local details in Figs.11 and 12, it is clear that NoiSER recovers the texture of the images more accurately and gets a better visual effect.

4.5. Automated Overexposure Suppression

Finally, we evaluate each method to process the overexposed image of SCIE dataset. As shown in Fig.13, existing methods, i.e., Zero-DCE [8], Zero-DCE++ [15], RUAS [18] and SCI [20], obtain poor results and the processed images are almost completely corrupted, since the aim of them is to learn a mapping from low to high illumination. One possible solution is to use a large scale multi-exposure dataset to train the model, so that the model can handle both overdark and overexposed images. However, it is still tricky to handle the extremely complex illumination in reality. Therefore, we are delighted to say that our NoiSER has an inborn ability to suppress the overexposure, since it learns a gray-world mapping which can automatically turn extreme light or dark into moderates, as shown in "NoiSER-Var3" in Fig.13.

5. Conclusion and Future Work

We have discussed a new problem, i.e., how to enhance a low-light image by deep learning without any task-related data? We have taken a bold and crazy perspective in thinking about the solution to the problem, but the final result offers plenty of surprises and amazing messages. We prove that the problem can easily solved by a simple and straightforward noise self-regression approach by learning a grayworld mapping. Extensive experiments demonstrate that our method yields a visually pleasing effect and obtains the competitive performance, in terms of strong learning ability, stable generalization capability, automated brightness adaptation and negligible computational consumption. In

the future, we will further think about how to optimize the noise for improving visual experience. In addition, we will prove our solution is easily embeddable and explore more possible applications by embedding our method to improve other low-level and high-level tasks in the dark.

6. Acknowledgment

This work is partially supported by the National Natural Science Foundation of China (62072151, 61932009, 61822701, 62036010, 72004174), and the Anhui Provincial Natural Science Fund for the Distinguished Young Scholars (2008085J30). Zhao Zhang is the corresponding author of this paper.

References

- [1] Gershon Buchsbaum. A spatial processor model for object colour perception. *Journal of the Franklin institute*, 310(1):1–26, 1980. 3
- [2] Jianrui Cai, Shuhang Gu, and Lei Zhang. Learning a deep single image contrast enhancer from multi-exposure images. *IEEE Trans. Image Process.*, 27(4):2049–2062, 2018. 8, 10, 13
- [3] Liangyu Chen, Xiaojie Chu, Xiangyu Zhang, and Jian Sun. Simple baselines for image restoration. *CoRR*, abs/2204.04676, 2022. 2
- [4] Ziteng Cui, Guo-Jun Qi, Lin Gu, Shaodi You, Zenghui Zhang, and Tatsuya Harada. Multitask AET with orthogonal tangent regularity for dark object detection. In *Proceedings* of the IEEE/CVF International Conference on Computer Vision, Montreal, QC, Canada, pages 2533–2542, 2021. 4
- [5] Dengxin Dai and Luc Van Gool. Dark model adaptation: Semantic image segmentation from daytime to nighttime. In Proceedings of the IEEE International Conference on Intelligent Transportation Systems, Maui, HI, USA, November 4-7, 2018, pages 3819–3824, 2018. 4
- [6] Ruicheng Feng, Chongyi Li, Shangchen Zhou, Wenxiu Sun, Qingpeng Zhu, Jun Jiang, Qingyu Yang, Chen Change Loy, and Jinwei Gu. MIPI 2022 challenge on under-display camera image restoration: Methods and results. *CoRR*, abs/2209.07052, 2022. 2
- [7] Ian J. Goodfellow, Jean Pouget-Abadie, Mehdi Mirza, Bing Xu, David Warde-Farley, Sherjil Ozair, Aaron C. Courville, and Yoshua Bengio. Generative adversarial networks. *Commun. ACM*, 63(11):139–144, 2020. 2
- [8] Chunle Guo, Chongyi Li, Jichang Guo, Chen Change Loy, Junhui Hou, Sam Kwong, and Runmin Cong. Zero-reference deep curve estimation for low-light image enhancement. In Proceedings of the IEEE/CVF Conference on Computer Vision and Pattern Recognition, Seattle, WA, USA, pages 1777–1786, 2020. 1, 2, 3, 9, 10, 11, 12, 13
- [9] Xiaojie Guo. LIME: A method for low-light image enhancement. In *Proceedings of the ACM Conference on Multime-dia Conference, Amsterdam, The Netherlands*, pages 87–91, 2016. 1, 9, 10, 11

- [10] Jiang Hai, Zhu Xuan, Ren Yang, Yutong Hao, Fengzhu Zou, Fang Lin, and Songchen Han. R2rnet: Low-light image enhancement via real-low to real-normal network. *CoRR*, abs/2106.14501, 2021. 8, 9, 10, 11, 12, 13
- [11] Geoffrey E Hinton and Ruslan R Salakhutdinov. Reducing the dimensionality of data with neural networks. *science*, 313(5786):504–507, 2006. 3
- [12] Yifan Jiang, Xinyu Gong, Ding Liu, Yu Cheng, Chen Fang, Xiaohui Shen, Jianchao Yang, Pan Zhou, and Zhangyang Wang. Enlightengan: Deep light enhancement without paired supervision. *IEEE Trans. Image Process.*, 30:2340–2349, 2021. 1, 2, 9, 10, 11, 12
- [13] Diederik P. Kingma and Jimmy Ba. Adam: A method for stochastic optimization. In *Proceedings of the International Conference on Learning Representations, San Diego, CA,* USA, 2015. 11
- [14] Diederik P. Kingma and Max Welling. Auto-encoding variational bayes. In *Proceedings of the International Conference* on Learning Representations, Banff, AB, Canada, 2014. 3
- [15] Chongyi Li, Chunle Guo, and Chen Change Loy. Learning to enhance low-light image via zero-reference deep curve estimation. *IEEE Trans. Pattern Anal. Mach. Intell.*, 44(8):4225–4238, 2022. 2, 3, 9, 10, 11, 12, 13
- [16] Dong Liang, Ling Li, Mingqiang Wei, Shuo Yang, Liyan Zhang, Wenhan Yang, Yun Du, and Huiyu Zhou. Semantically contrastive learning for low-light image enhancement. In *Proceedings of the AAAI Conference on Artificial Intelli*gence, Virtual, pages 1555–1563, 2022. 3
- [17] Jinxiu Liang, Jingwen Wang, Yuhui Quan, Tianyi Chen, Jiaying Liu, Haibin Ling, and Yong Xu. Recurrent exposure generation for low-light face detection. *IEEE Trans. Multim.*, 24:1609–1621, 2022. 4
- [18] Risheng Liu, Long Ma, Jiaao Zhang, Xin Fan, and Zhongxuan Luo. Retinex-inspired unrolling with cooperative prior architecture search for low-light image enhancement. In *Proceedings of the IEEE Conference on Computer Vision and Pattern Recognition, virtual*, pages 10561–10570, 2021. 1, 2, 9, 10, 11, 12, 13
- [19] Kin Gwn Lore, Adedotun Akintayo, and Soumik Sarkar. Llnet: A deep autoencoder approach to natural low-light image enhancement. *Pattern Recognit.*, 61:650–662, 2017. 2
- [20] Long Ma, Tengyu Ma, Risheng Liu, Xin Fan, and Zhongxuan Luo. Toward fast, flexible, and robust low-light image enhancement. In *Proceedings of the IEEE/CVF Conference* on Computer Vision and Pattern Recognition, New Orleans, LA, USA, pages 5627–5636, 2022. 2, 9, 10, 11, 12, 13
- [21] Candy McCabe. Mirror visual feedback therapy. a practical approach. *Journal of hand therapy*, 24(2):170–179, 2011. 3
- [22] Anish Mittal, Rajiv Soundararajan, and Alan C. Bovik. Making a "completely blind" image quality analyzer. *IEEE Signal Process. Lett.*, 20(3):209–212, 2013. 10
- [23] Seungjun Nah, Tae Hyun Kim, and Kyoung Mu Lee. Deep multi-scale convolutional neural network for dynamic scene deblurring. In *Proceedings of the IEEE Conference on Computer Vision and Pattern Recognition, Honolulu, HI, USA*, pages 257–265, 2017. 2

- [24] Adam Paszke, Sam Gross, Francisco Massa, Adam Lerer, James Bradbury, Gregory Chanan, Trevor Killeen, Zeming Lin, Natalia Gimelshein, Luca Antiga, Alban Desmaison, Andreas Köpf, Edward Z. Yang, Zachary DeVito, Martin Raison, Alykhan Tejani, Sasank Chilamkurthy, Benoit Steiner, Lu Fang, Junjie Bai, and Soumith Chintala. Pytorch: An imperative style, high-performance deep learning library. In Proceedings of the Advances in Neural Information Processing Systems, Vancouver, BC, Canada, pages 8024–8035, 2019. 10
- [25] Joseph Redmon, Santosh Kumar Divvala, Ross B. Girshick, and Ali Farhadi. You only look once: Unified, real-time object detection. In *Proceedings of the IEEE Conference on Computer Vision and Pattern Recognition, Las Vegas, NV, USA*, pages 779–788, 2016. 2
- [26] Jiahuan Ren, Zhao Zhang, Richang Hong, Mingliang Xu, Yi Yang, and Shuicheng Yan. Seeing through the noisy dark: Toward real-world low-light image enhancement and denoising. *CoRR*, abs/2210.00545, 2022. 3
- [27] Olaf Ronneberger, Philipp Fischer, and Thomas Brox. Unet: Convolutional networks for biomedical image segmentation. In *Proceedings of the Medical Image Computing and Computer-Assisted Intervention, Germany*, volume 9351, pages 234–241, 2015. 2
- [28] Dmitry Ulyanov, Andrea Vedaldi, and Victor S. Lempitsky. Deep image prior. In Proceedings of the IEEE Conference on Computer Vision and Pattern Recognition, Salt Lake City, UT, USA, pages 9446–9454, 2018. 3
- [29] Yecong Wan, Yuanshuo Cheng, Mingwen Shao, and Jordi Gonzàlez. Image rain removal and illumination enhancement done in one go. *Knowl. Based Syst.*, 252:109244, 2022. 3
- [30] Wenjing Wang, Xinhao Wang, Wenhan Yang, and Jiaying Liu. Unsupervised face detection in the dark. *IEEE Trans. Pattern Anal. Mach. Intell.*, 2022. 4
- [31] Wenjing Wang, Wenhan Yang, and Jiaying Liu. Hla-face: Joint high-low adaptation for low light face detection. In *Proceedings of the IEEE Conference on Computer Vision and Pattern Recognition, virtual*, pages 16195–16204, 2021. 1, 4
- [32] Zhou Wang, Alan C. Bovik, Hamid R. Sheikh, and Eero P. Simoncelli. Image quality assessment: from error visibility to structural similarity. *IEEE Trans. Image Process.*, 13(4):600–612, 2004. 10
- [33] Chen Wei, Wenjing Wang, Wenhan Yang, and Jiaying Liu. Deep retinex decomposition for low-light enhancement. In *Proceedings of the British Machine Vision Conference, New-castle, UK*, page 155, 2018. 1, 8, 9, 10, 11, 12
- [34] Yanyan Wei, Zhao Zhang, Yang Wang, Mingliang Xu, Yi Yang, Shuicheng Yan, and Meng Wang. Deraincyclegan: Rain attentive cyclegan for single image deraining and rainmaking. *IEEE Trans. Image Process.*, 30:4788–4801, 2021.

- [35] Ke Xu, Xin Yang, Baocai Yin, and Rynson W. H. Lau. Learning to restore low-light images via decomposition-andenhancement. In Proceedings of the IEEE/CVF Conference on Computer Vision and Pattern Recognition, Seattle, WA, USA, pages 2278–2287, 2020. 2
- [36] Syed Waqas Zamir, Aditya Arora, Salman H. Khan, Munawar Hayat, Fahad Shahbaz Khan, Ming-Hsuan Yang, and Ling Shao. Multi-stage progressive image restoration. In Proceedings of the IEEE Conference on Computer Vision and Pattern Recognition, virtual, pages 14821–14831, 2021.
- [37] Qing Zhang, Yongwei Nie, and Wei-Shi Zheng. Dual illumination estimation for robust exposure correction. *Comput. Graph. Forum*, 38(7):243–252, 2019. 1, 9, 10, 11
- [38] Yonghua Zhang, Xiaojie Guo, Jiayi Ma, Wei Liu, and Jiawan Zhang. Beyond brightening low-light images. *Int. J. Comput. Vis.*, 129(4):1013–1037, 2021.
- [39] Yonghua Zhang, Jiawan Zhang, and Xiaojie Guo. Kindling the darkness: A practical low-light image enhancer. In Proceedings of the ACM International Conference on Multimedia, Nice, France, pages 1632–1640, 2019.
- [40] Zhao Zhang, Huan Zheng, Richang Hong, Mingliang Xu, Shuicheng Yan, and Meng Wang. Deep color consistent network for low-light image enhancement. In *Proceedings* of the IEEE/CVF Conference on Computer Vision and Pattern Recognition, New Orleans, LA, USA, pages 1889–1898, 2022. 1, 2
- [41] Suiyi Zhao, Zhao Zhang, Richang Hong, Mingliang Xu, Yi Yang, and Meng Wang. FCL-GAN: A lightweight and real-time baseline for unsupervised blind image deblurring. In *Proceedings of the ACM International Conference on Multimedia, Lisboa, Portugal*, pages 6220–6229, 2022. 2
- [42] Suiyi Zhao, Zhao Zhang, Richang Hong, Mingliang Xu, Haijun Zhang, Meng Wang, and Shuicheng Yan. Crnet: Unsupervised color retention network for blind motion deblurring. In *Proceedings of the ACM International Conference* on Multimedia, Lisboa, Portugal, pages 6193–6201, 2022. 2
- [43] Yuzhi Zhao, Yongzhe Xu, Qiong Yan, Dingdong Yang, Xuehui Wang, and Lai-Man Po. D2hnet: Joint denoising and deblurring with hierarchical network for robust night image restoration. *CoRR*, abs/2207.03294, 2022. 1
- [44] Jun-Yan Zhu, Taesung Park, Phillip Isola, and Alexei A. Efros. Unpaired image-to-image translation using cycle-consistent adversarial networks. In *Proceedings of the IEEE International Conference on Computer Vision, Venice, Italy*, pages 2242–2251, 2017. 2
- [45] Fuzhen Zhuang, Zhiyuan Qi, Keyu Duan, Dongbo Xi, Yongchun Zhu, Hengshu Zhu, Hui Xiong, and Qing He. A comprehensive survey on transfer learning. *Proc. IEEE*, 109(1):43–76, 2021. 4